Projected Changes in Mean and Extreme Precipitation in Africa under Global Warming. Part I: Southern Africa

M. E. SHONGWE,* G. J. VAN OLDENBORGH, AND B. J. J. M. VAN DEN HURK

Royal Netherlands Meteorological Institute, De Bilt, Netherlands

B. DE BOER

Institute for Marine and Atmospheric Research, Utrecht University, Utrecht, Netherlands

C. A. S. COELHO

Centro de Previsão de Tempo e Estudos Climáticos, Instituto Nacional de Pesquisas Espaciais, Cachoeira Paulista, Brazil

M. K. VAN AALST

Red Cross/Red Crescent Climate Centre, The Hague, Netherlands

(Manuscript received 7 November 2007, in final form 29 January 2009)

ABSTRACT

This study investigates likely changes in mean and extreme precipitation over southern Africa in response to changes in radiative forcing using an ensemble of global climate models prepared for the Intergovernmental Panel on Climate Change (IPCC) Fourth Assessment Report (AR4). Extreme seasonal precipitation is defined in terms of 10-yr return levels obtained by inverting a generalized Pareto distribution fitted to excesses above a predefined high threshold. Both present (control) and future climate precipitation extremes are estimated. The future-to-control climate ratio of 10-yr return levels is then used as an indicator for the likely changes in extreme seasonal precipitation.

A Bayesian approach to multimodel ensembling is adopted. The relative weights assigned to each of the model simulations is determined from bias, convergence, and correlation. Using this method, the probable limits of the changes in mean and extreme precipitation are estimated from their posterior distribution.

Over the western parts of southern Africa, an increase in the severity of dry extremes parallels a statistically significant decrease in mean precipitation during austral summer months. A notable delay in the onset of the rainy season is found in almost the entire region. An early cessation is found in many parts. This implies a statistically significant shortening of the rainy season.

A substantial reduction in moisture influx from the southwestern Indian Ocean during austral spring is projected. This and the preaustral spring moisture deficits are possible mechanisms delaying the rainfall onset in southern Africa. A possible offshore (northeasterly) shift of the tropical–temperate cloud band is consistent with more severe droughts in the southwest of southern Africa and enhanced precipitation farther north in Zambia, Malawi, and northern Mozambique.

This study shows that changes in the mean vary on relatively small spatial scales in southern Africa and differ between seasons. Changes in extremes often, but not always, parallel changes in the mean precipitation.

1. Introduction

Changes in the mean state of the earth's climate system due to anthropogenic modifications in the chemical composition of the earth's atmosphere have become a topical issue in recent years (Houghton et al. 2001; Solomon et al. 2007). Direct consequences of positive radiative forcing resulting from an enhanced greenhouse effect are changes in global surface and

* Additional affiliation: Swaziland National Meteorological Service, Mbabane, Swaziland.

Corresponding author address: Mxolisi E. Shongwe, KNMI, P.O. Box 201, 3730 AE, De Bilt, Netherlands.
E-mail: mxolisi.shongwe@knmi.nl

DOI: 10.1175/2009JCLI2317.1

© 2009 American Meteorological Society

atmospheric temperatures, precipitation patterns, and other climate variables (Solomon et al. 2007).

Owing to their great impact on human activity and wide application, potential future changes in precipitation deserve much attention. A number of studies have sought the possible changes in long-term mean precipitation in many parts of the globe (Giorgi and Mearns 2002, 2003; Trenberth et al. 2003; Tebaldi et al. 2004). Less attention has been paid to changes in extreme precipitation. Pronounced increases in heavy precipitation events might be expected to occur where mean total seasonal or annual precipitation increases. On the other hand, dry extremes might be expected to become severe where mean precipitation decreases. However, in cases where the interannual rainfall variance increases, it is possible that changes in the probability of extreme precipitation events may not parallel that of mean seasonal or annual precipitation. For instance, the severity of heavy precipitation events may increase in regions where the total precipitation decreases or remains constant. Since precipitation extremes often have bigger impacts on society than small changes in average precipitation, an investigation of extreme behavior under changing climatic conditions is warranted.

Several studies have investigated the likely changes in mean and extreme precipitation in many parts of the globe, including Africa (Kharin and Zwiers 2000; Groisman et al. 2005; Meehl et al. 2005; Kharin et al. 2007). Most of these studies have focused on likely patterns of change over large regions of Africa despite the high degree of spatial variability exhibited by precipitation. Regionally specific studies have been carried out in other parts of the globe (e.g., van Ulden and van Oldenborgh 2006; van den Hurk et al. 2006), but few for Africa and even fewer for southern Africa.

Hulme et al. (2001) reviewed previous African climate change studies and report on observed (twentieth century) and likely future (twenty-first century) mean annual temperature and precipitation patterns in Africa. Using seven global climate models (GCMs), significant decreases in mean December–February (DJF) precipitation were found in the interior southern Africa south of about 10°S (most of South Africa, Botswana, and Namibia) in the A2-high scenario. These projected decreases are substantial after 2050 (their Fig. 10). Sources of uncertainty in African climate change scenario studies are also discussed (Hulme et al. 2001). Previous southern African climate change studies investigating extreme events (e.g., Joubert et al. 1996; Mason et al. 1999) used either simulations by a single climate model or earlier version(s) of a few climate models. Using an earlier version of the Commonwealth Scientific and Industrial Research Organisation (CSIRO) coupled general circulation model (CGCM), Joubert et al. (1996) found an increase in the probability of dry years over the southwestern parts of southern Africa and southern Mozambique under $2 \times CO_2$ experiments. However, southern African mean annual precipitation was not found to change significantly. Mason et al. (1999) found an increase in the frequency of extremely wet daily events. Consistent with Joubert et al., no significant trend in mean annual precipitation was reported. Here, we conduct a detailed regional analysis by combining results from an ensemble of objectively selected state-of-the-art climate models to investigate likely long-term (up to 2200) changes in mean and extreme precipitation.

Over the past decades, climate-related extremes have been the dominant trigger of natural disasters in southern Africa (here defined as Botswana, Lesotho, Malawi, Mozambique, Namibia, South Africa, Swaziland, Zambia, and Zimbabwe). New et al. (2006) identified significant trends in southern Africa temperature extremes and some precipitation indices. In particular, a spatially coherent increase in consecutive dry days was found over much of southern Africa in the last decades of the twentieth century. Upward trends in intense precipitation were found to the southeast with trends of the opposite sign in northern Namibia, Botswana, and Zambia.

Concurrently, the number of disasters is on the rise. According to the International Emergency Disasters Database (EM-DAT; http://www.em-dat.net/), the average annual number of reported natural disasters in the region has risen from about 5 reported disasters a year in the 1980s to over 18 a year from 2000 to 2006. Hydrometeorological disasters make up the bulk of those (the others are mostly epidemics such as malaria, cholera, and meningitis, which are also affected by climatic conditions). Reported drought-related disasters have risen from an average of about 1.5 per year in the 1980s to about 2 per year since 2000, while those related to floods have risen from 1.2 a year to almost 7 per year since 2000 (the rest of the reported increase is mainly due to wind storms). In the past years, these events have affected the lives and livelihoods of over six million people annually and had severe impacts on economic performance and poverty alleviation (e.g., Hellmuth et al. 2007). While part of the trend is due to better reporting, it also reflects a rising vulnerability to natural hazards, and potentially an underlying trend in climate variability and extremes. Operational disaster managers, for instance from the Red Cross and Red Crescent, also report an increasing pressure on humanitarian assistance and express concern that trends in weather extremes due to climate change increasingly affect their work (e.g., van Aalst et al. 2007). Among others, they

are looking for better analyses on how extreme weather events may be changing so as to enhance disaster preparedness among poor rural communities and help integrate climate risk management into development planning. These concerns and questions have provided the motivation for the present study.

Of particular interest is examining likely changes from the present to the late twenty-first and twenty-second centuries (i.e., the 2051–2200 period) in the severity of droughts and floods in specific regions of Africa and a comparison with changes in mean precipitation. With the vulnerable local communities and high spatial variation of rainfall in mind, this study probes into simulated precipitation changes at spatial scales smaller than the commonly used Giorgi regions (Giorgi and Francisco 2000). Here, we show that averaging over large areas can conceal notable spatial variations in the modeled rainfall response to an enhanced greenhouse effect. Likely changes in large-scale atmospheric hydrodynamics are assessed and related to changes in precipitation patterns. Results obtained for southern Africa are presented in this paper. A companion paper (Shongwe et al. 2008, manuscript submitted to *J. Climate*) presents the results for East Africa. In spite of the associated uncertainties (e.g., Hulme et al. 2001), the results presented below can inform adaptation strategies for governments, the private sector, and communities in the regions covered in this study.

2. Data and methods

a. Model simulations and observations

This study uses the World Climate Research Programme (WCRP) Coupled Model Intercomparison Project phase 3 (CMIP3) multimodel dataset. The model dataset formed input to the Intergovernmental Panel on Climate Change (IPCC) Fourth Assessment Report (AR4) (Solomon et al. 2007). Correlation between modeled and Climate Research Unit (CRU) monthly precipitation and the rms error (RMSE) is used to assess the degree of realism with which models available on the Program for Climate Model Diagnosis and Intercomparison (PCMDI) archive simulate the observed twentieth-century precipitation (the 20c3m runs). With this first low-threshold selection, 12 models were selected and are listed in Table 1. For details of each model formulation, the reader is referred to the references cited in the table. The model spatial resolutions differ considerably. As the focus of this study is on relatively small spatial scales, for ease of comparison, the model simulations are linearly interpolated to a common T95 ($1.25° \times \sim 1.24°$ latitude–longitude) grid.

The availability of long integrations from the Special Report on Emissions Scenarios (SRES) A1B forced runs enable the assessment of possible long-term climate change signals. In this scenario, CO_2 concentration doubles by 2100 and remains constant thereafter. These SRESA1b model data are subdivided into two subsamples: the 1901–2000 and the 2051–2200 periods, defining the control and future climate, respectively. Considering the 2051–2200 period is sensible because, in most cases, changes in model predictions before and after 2100 (CO_2 doubling) are smaller than the internal variability. For climate models with multiple integrations (n20c3m and nSRESA1b; Table 1), each ensemble member is considered an independent realization. The ensemble members are then concatenated to form a larger sample for each model from which further analyses (see section 2c) are carried out.

To identify the atmospheric anomalies and/or moisture attributes associated with precipitation changes, other fields (e.g., wind and specific humidity) from the model simulations are also used. The computation of moisture transport, for example, requires data on finer temporal resolution than the monthly simulations used to estimate precipitation changes. Daily simulations from the same CGCMs listed in Table 1 are used, except for the third climate configuration of the Met Office Unified Model (HadCM3) and Hadley Centre Global Environmental Model version 1 (HadGEM1), whose data is not available on the PCMDI archive. The PCMDI archive contains only daily data for shorter time slices (e.g., 1961–2000, 2046–65, and 2081–2100) and, therefore, the analysis of these quantities will be based on these shorter periods.

Observed twentieth-century precipitation data used in this study comprise station observations obtained from the Global Historical Climatology Network (GHCN) (Peterson et al. 1997) and gridded data from the Climate Research Unit (CRU TS2.1) (New et al. 2000) datasets. The former is only used to define homogeneous rainfall regions (see section 2b). The latter is used in all analyses described in sections 2c and 2d. The biases inherent in these datasets notwithstanding, their quality is sufficient for the present study.

Prior to the analysis of precipitation changes, the data have been screened for possible trends. Except for clear patterns of low-frequency precipitation variability in some regions, significant twentieth-century precipitation trends are not discernible. Detrending the series prior to the analysis is therefore deemed unnecessary. The mean seasonal precipitation rates used here are separated by 12 months. Clusters of extremes may only reflect interdecadal variability rather than serial dependence. For this reason, declustering the time series has also been deemed unnecessary.

TABLE 1. Global coupled climate models used in this study. Model resolution is given as T (wavenumber of spectral truncation) and L (number of vertical layers). The number of ensemble integration by each model in the twentieth century and future climate (2051–2200) climate are shown in the columns with headings n20c3m and nSRESA1b, respectively.

Contributing center	Model	Atmospheric resolution	nSRESA		References
			n20c3m	1b	
Canadian Centre for Climate Modelling and Analysis (CCCMA)	General Circulation Model version 3.1 (GCM3.1) (T47)	T47L31	5	5	Flato (2005)
Météo-France	CNRM-CM3	T42L45	1	1	Salas-Mélia et al. (2005)
CSIRO	CSIRO Mark version 3.0 (Mk3.0)	T63L18	3	1	Gordon et al. (2002)
Max Planck Institute (MPI)	ECHAM5/MPI Ocean Model (OM)	T63L31	3	3	Roeckner et al. (2003)
Meteorological Institute of the University of Bonn (MIUB)	ECHO-G	T30L19	3	3	Min et al. (2005)
GFDL	GFDL CM2.0	2° × 2.5° L24	3	1	Delworth et al. (2006)
GFDL	GFDL CM2.1	2° × 2.5° L24	3	1	Delworth et al. (2006)
L'Institut Pierre-Simon Laplace (IPSL)	IPSL Coupled Model, version 4 (CM4)	2.5° × 3.75° L30	1	1	Le Clainche et al. (2001)
Center for Climate System Research/National Institute for Environmental Studies/Frontier Research Center for Global Change (CCSR/NIES/ FRCGC)	Model for Interdisciplinary Research on Climate 3.2, medium-resolution version [MIROC3.2 (medres)]	T42L20	3	1	Hasumi et al. (2004)
MRI	MRI CGCM2.3.2	T42L30	5	1	Yukimoto and Noda (2001)
Met Office (UKMO)	UKMO HadCM3	2.5° × 3.75° L19	2	1	Gordon et al. (2000)
UKMO	UKMO HadGEM1	1.25° × 1.875° L38	2	1	Johns et al. (2004)

Because of its geographical diversity, Africa is divided into four subregions: southern Africa, East Africa, northeast Africa, and West Africa. As aforementioned, this paper present results obtained for southern Africa (defined here as the area lying between ~35° and 10°S, 20° and 42°E; Fig. 1). Results for other regions are presented online at http://www.knmi.nl/africa_scenarios/. Because of sparsity of reliable observations in certain parts of southern Africa (e.g., Angola and Democratic Republic of Congo), these areas have been omitted from the analysis.

Much of southern Africa has a well-defined rainy season during austral summer months and is characterized by distinct atmospheric dynamics (Tyson and Preston-Whyte 2000). In this study, future patterns of southern Africa mean precipitation change in austral spring [September–November (SON)], summer [December–February (DJF)], autumn [March–May (MAM)], and winter [June–August (JJA)] are investigated. Extreme precipitation change analysis is only carried out for the peak of summer (DJF), when most precipitation and extreme events typically occur (Tyson and Preston-Whyte 2000). Monthly CRU and CMIP3 precipitation is accumulated into seasonal (3 month) totals from which mean daily precipitation rates are calculated by dividing by the number of days in that season. The climatologically wettest seasons have the highest mean precipitation rates—from either a few very intense rainfall events or prolonged wet spells within that season. On the other hand, the driest seasons (drought events) have the lowest mean precipitation rates.

b. *Clustering stations*

Mean precipitation and return levels (section 2c) exhibit pronounced spatial variabilities. This is largely in response to inhomogeneities in land surface features (e.g., topography and land–sea–lake contrasts). Such localized forcing features are expected to modulate the precipitation response to changes in radiative forcing. For this reason, using the GHCN data, homogeneous rainfall regions are identified within southern Africa using cluster analysis (Mimmack et al. 2001). Rainfall homogeneity is defined on the basis of the spatial coherence of interannual rainfall variations.

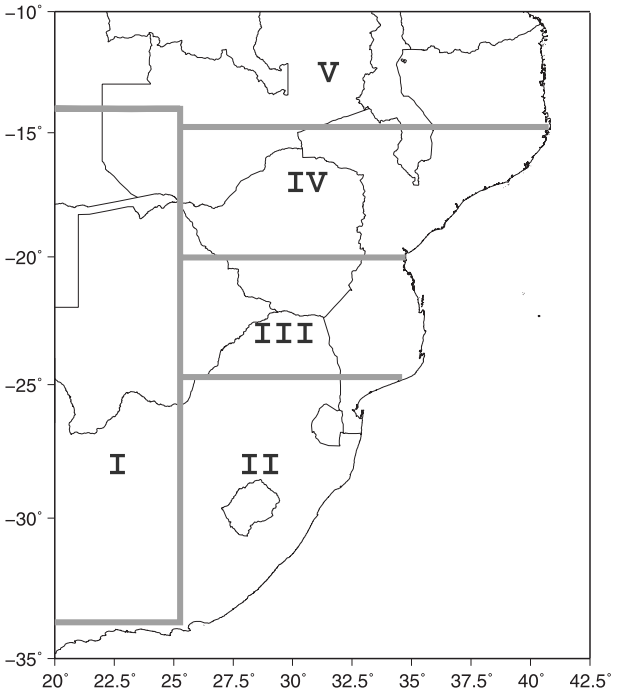

FIG. 1. Location map of the southern Africa climatic zones identified using Ward's minimum variance clustering method.

Prior to the clustering, annual precipitation totals are first calculated using the July–June year. The annual totals are then clustered using single linkage, average linkage, complete linkage, and Ward's agglomerative hierarchical algorithms (Johnson and Wichern 2002). Each hierarchical procedure is based on Euclidean distances between station rainfall data, standardized by removing the mean and dividing by the mean absolute deviations.

Of the clustering methods used, the Ward minimum error sum of squares procedure yielded the most sensible results. The results from average linkage and complete linkage methods are broadly similar to those from Ward's method. Poorly separated clusters representing less distinct regions are merged if the regions are contiguous. In addition, transitions between regions have been smoothed and straight lines used to delineate region boundaries. For these reasons, the resulting climate regions shown in Fig. 1 differ from those identified by Shongwe et al. (2006). Here we used 212 stations spanning the period 1941–97 in contrast to the 255 stations and shorter period (1961–2000) used previously (Shongwe et al. 2006). Furthermore, in Shongwe et al., the clustering was based on Euclidean distances calculated from unstandardized principal component scores of individual monthly rainfall data, as recommended by Mimmack et al. (2001).

Observed seasonal precipitation for each homogeneous zone is calculated from the CRU datasets by averaging grid points that fall within it. Gridded CRU precipitation data, which is based on the GHCN station data and automatically gives equal weight to equal areas, is preferred for further analysis (see sections 2c and 2d below). CGCM grids falling within each climatic zone were similarly averaged. In this way, the spatial noise inherent in precipitation has been filtered out.

c. *Extreme value analysis*

The analysis of changes of extreme precipitation events is based on the peak-over-threshold method or generalized Pareto distribution (GPD). In contrast to using the raw (model) data, fitting a GPD allows interpolation, extrapolation, and intermodel comparison. A comprehensive introduction to GPD and its applications can be found in Coles (2001). Details of the extreme value model applied here are presented in appendix A.

Conventionally, most extreme value studies in climate science (e.g., Kharin and Zwiers 2000; Meehl et al. 2005; Kharin et al. 2007) evaluate return levels or quantiles of a GPD. In this study, 10-, 20-, 50-, and 100-yr return levels have been estimated. However, given the small sample size of threshold excesses, only the 10-yr return levels are shown. These estimates are interpolated from the data, rather than extrapolated, and hence are least biased. Results for longer return levels are available online at http://www.knmi.nl/africa_scenarios/. Ten-year return levels (mm day^{-1}) are computed in both control and future climate. These levels express the average intensity of precipitation in an extremely wet or dry season that occurs on average once every 10 years (corresponding to 10% probability that a given season is wetter or drier than this).

Anderson–Darling goodness-of-fit tests (Laio 2004) have been used to assess the suitability of the GPD as a model of excesses above the predefined threshold. The mathematical formulation of this test is shown in appendix B. The test statistics and critical values are determined from the National Institute of Standards and Technology software available online at http://www.itl.nist.gov/div898/software/dataplot.html/.

d. *Multimodel ensembling*

Uncertainties in long-term climate model simulations can be classified as those due to natural climate variability, model different responses to a given forcing (such as increases in greenhouse gas concentration), model imperfections under the control forcing, and those associated with the emission scenarios used to force the climate models. For these reasons, no single model is

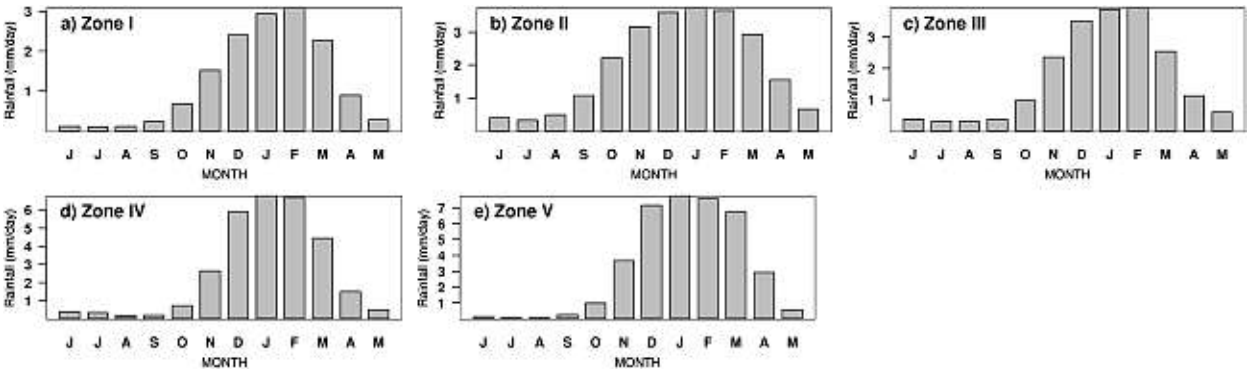

FIG. 2. Annual cycle of southern Africa precipitation derived from the 1901–2000 CRU gridded data. Zone labels are as indicated in Fig. 1.

considered accurate. Many climate studies utilize results from a range of climate models (e.g., Kharin et al. 2007).

Considerable research is devoted to methods for combining simulations from climate models (e.g., Giorgi and Mearns 2002, 2003; Tebaldi et al. 2004, 2005). This paper adopts the Bayesian method defined by Tebaldi et al. (2005). The inherent advantage of this method is that uncertainties of the measures of interest can be inferred from their posterior distributions, which combines simulation information from all climate models. This method uses model bias, convergence between model projections, and correlation to determine the relative weights given to each member in the multimodel ensemble. Model bias is defined with respect to the twentieth-century climate, whereas convergence measures the distance of the individual model projection from the location of the multimodel ensemble. Models that simulate the observed climate with some skill and agree with the rest in their future projections receive more weight. On the other hand, outliers, which show large biases with respect to the observed climate, are weighted least. Correlation between the individual model's deviations from the multimodel ensemble mean in the present and future climate is also incorporated in the weighting criteria. In this way, models with systematic biases are further downweighted. The bias and convergence criteria for determining weights assigned to each member in the ensemble has been applied previously (Giorgi and Mearns 2002, 2003). No specific criteria for assigning weights to model predictions can be considered optimal. For instance, it is quite possible that several models that exhibit similar performance in simulating the observed twentieth-century climate still produce quite different projections for the future climate. The risk of discounting the best model when it is an outlier with respect to the rest is inevitable from the convergence criterion. Notwithstanding, these weighting criteria bear enough theoretical and statistical basis to justify their use.

Fuller details of the statistical treatment of the problem may be found in Tebaldi et al. (2005). Here, adopting their notation, it suffices to show the measure of percentage precipitation change as

$$\Delta P = 100\left(\frac{\nu}{\mu} - 1\right), \tag{1}$$

where ν and μ are used to designate the mean of the multimodel ensemble in the future and control climate, respectively. For mean precipitation rates and 10-yr wettest events, $\Delta P > 0$ is indicative of an increase in their intensity, while an increase in the severity of 10-yr driest events is indicated by $\Delta P < 0$.

3. Projected precipitation changes

Mean precipitation in each month computed from the twentieth-century (1901–2000) CRU gridded data, spatially averaged over each zone, is shown in Fig. 2. Almost everywhere in the region, seasonal rainfall commences around austral spring months (SON) and ceases around autumn months (MAM). DJF is the peak of the rainfall season, while JJA is typically dry (less than 1 mm day^{-1}).

This section begins by presenting likely changes in mean precipitation during transition seasons. We then discuss the projected changes in mean and extreme precipitation during the peak summer months (DJF). Projected changes in winter precipitation, which are of little social and economical significance, are shown in section 4a.

To allow a concise visual interpretation, we present the results for the percentage change in precipitation [ΔP, Eq. (1)] for each climatic zone (Fig. 1) as the mean change with the corresponding 95% confidence interval derived from the Bayesian method. In each case, statistical significance at the 5% level (i.e., $p < 0.05$) is

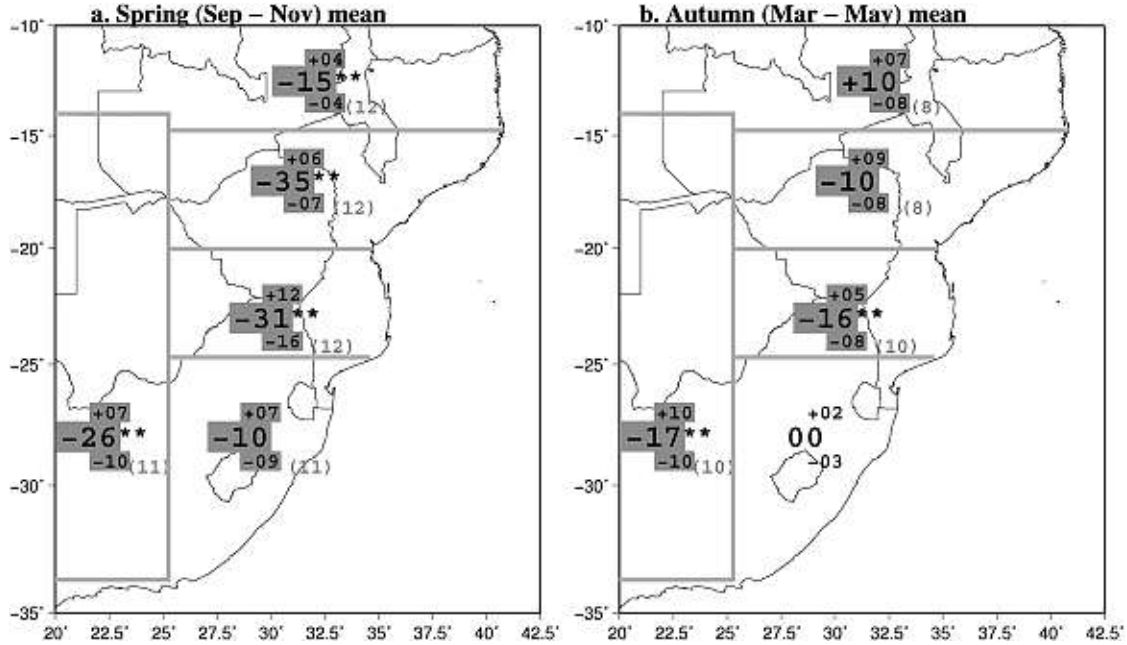

FIG. 3. Projected changes (%) in austral (a) spring (Sep–Nov) and (b) autumn (Mar–May) mean daily precipitation rates in each climatic zone. In each case, three values are plotted. The middle number gives the mean projected change preceded by its sign (+ve for increase and −ve for decrease). The number above (below) the mean change, preceded by a +ve (−ve) sign, gives the distance to the upper (lower) critical value at the 5% level of significance. Projected changes significant at the 5% (1%) level are shaded in gray (shown by two asterisks). For statistically significant changes, the number of CGCMs (out of 12) projecting a change of the same sign as the mean change is enclosed in parentheses.

found whenever the 95% confidence region excludes zero (i.e., the null hypothesis of no change). Significance at the 1% level ($p < 0.01$) is also tested. Whenever statistical significance in the projected changes is achieved, the number of CGCMs (out of the 12) projecting a change of the same sign as the mean change is shown. This is to demonstrate that the Bayesian weighting procedure is not doing anything weird.

a. Changes in the transition season mean precipitation

A spatially coherent and significant reduction ($p < 0.05$) in austral spring (SON) mean precipitation is found everywhere in southern Africa (Fig. 3a). Reductions in SON precipitation have implications for seasonal rainfall onset in southern Africa. To the west (zone I) and over Zimbabwe and central Mozambique, a reduction exceeding 20% is simulated with the lower bound of the 95% posterior interval of $\Delta P < -35\%$. Almost everywhere in the region, the entire range of percentage reduction in SON precipitation excludes zero, indicative of a considerable consensus across the models. This, together with spatial coherence of this pattern of change, strengthens the belief that this is a consistently modeled climate change signal. Tadross et al. (2005) present the climatology of rainfall onset in southern Africa. Areas to the south experience an earlier rainfall onset from extratropical circulation systems such as frontal depressions and cold-core cutoff lows (Tyson and Preston-Whyte 2000). Albeit relatively small (~10%), the simulated SON precipitation decrease over eastern South Africa (zone II) is significant. To the north and west, where precipitation is predominantly of tropical origin (Tyson and Preston-Whyte 2000), reduction in spring precipitation attains significance at the 1% level.

Projected changes in mean autumn (MAM) precipitation rates are displayed in Fig. 3b. Over zones I and III (much of Botswana and southern Zimbabwe), the simulated mean reduction of ~15% attains statistical significance at the 1% level. In zone IV (northern Zimbabwe and central Mozambique), the mean reduction (~10%) is barely significant at the 5% level. Considering that a notable delay in rainfall onset is simulated in these areas, projections for an early cessation of seasonal rains suggest a contraction of the rainfall season. Farther north, in zone V (northern Mozambique, Zambia, and Malawi), MAM precipitation is expected to increase by ~10%. A shift in the rainfall season to later months is implied. Little or no change in MAM precipitation

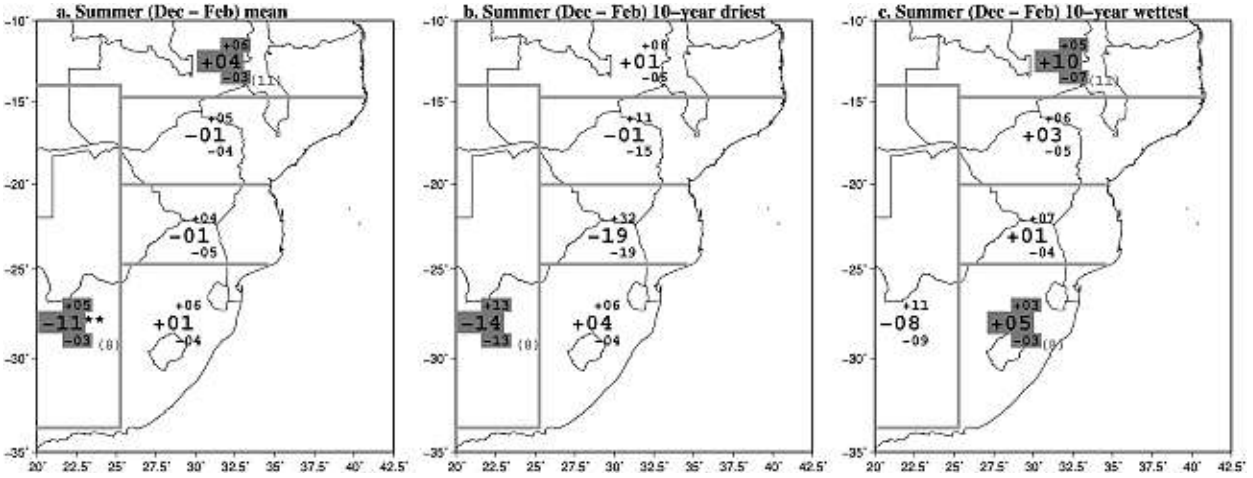

FIG. 4. As in Fig. 3, but for austral summer (Dec–Feb): (a) mean precipitation rates, (b) 10-yr driest events, and (c) 10-yr wettest events.

is projected in eastern South Africa, which implies a shortening of the rainy season.

b. Changes in mean and extreme summer precipitation rates

Figure 4 displays probable changes in summer (DJF) precipitation rates. There is evidence for a dipole pattern of change in mean precipitation rates (Fig. 4a). The negative pole is found to the western parts featuring the arid Kalahari and its boundaries (zone I). Here, the projected reduction in DJF mean precipitation rates (~11%) is significant at the 1% level. Farther north, in the positive pole (zone V), the simulated changes, albeit subtle (~4%), are significant at the 5% level. Separating the dipole is a large area to the east (zones II, III, and IV) with no significant changes in mean DJF precipitation rates. The presence of a dipole precipitation response to large-scale forcing (e.g., El Niño; Ropelewski and Halpert 1987) has been found at interannual time scales. Its appearance here suggests that the climate change signal propagates into the southern Africa precipitation field through similar pathways (e.g., the tropical Indian Ocean SST pathway, Goddard and Graham 1999; Washington and Preston 2006).

Over the western parts of the subregion, 10-yr driest seasons are projected to increase their severity by more than 10% (Fig. 4b). These projections are significant at the 5% level. More severe droughts are also projected to the south of Zimbabwe and Mozambique. Albeit high in magnitude (averaging ~20%), these projections are not statistically significant. Elsewhere in the region, the models give little or no indications for a possible change in 10-yr driest events. Anomalous westerly circulations over the southeast Atlantic Ocean have been blamed for past droughts in much of southwestern Africa (Mulenga et al. 2003). The anomalous circulation patterns are related to the structure of the tropical–temperate cloud bands (Todd and Washington 1999). We postulate that these mechanisms might be present with similar consequences in the future climate. We shall return to this point in section 4b.

Subtle but generally significant increases in 10-yr wettest events are found in eastern South Africa and farther north in northern Zambia, Malawi, and Mozambique (Fig. 4c). In the north, the magnitude of these changes average ~10%. A slight and insignificant decrease in the intensity of 10-yr wettest events is projected in the western parts of southern Africa (Botswana and western South Africa: zone I). Elsewhere in the east (zones III and IV), subtle and insignificant increases are found. In the southern and eastern parts of the study area, flooding has often occurred from short-duration mesoscale events such as depressions (e.g., Rouault et al. 2002) and cutoff lows and by landfalling west Indian Ocean tropical cyclones (e.g., Reason and Keibel 2004; Reason 2007). While there are indications of possible changes in the intensity of the 10-yr wettest events, poor representation of small-scale systems (e.g., tropical cyclone activity) in CGCMs limit the confidence we have in these projected changes. The northern areas (zone V) are least affected by west Indian Ocean tropical storms. In these regions, wettest seasons are associated with prolonged sequences of wet days, which are dependent on the mean location and strength of large-scale convection. The projected changes in these regions are therefore more reliable.

The observed (1901–2000) and simulated (1901–2100) DJF precipitation time series for each zone are displayed

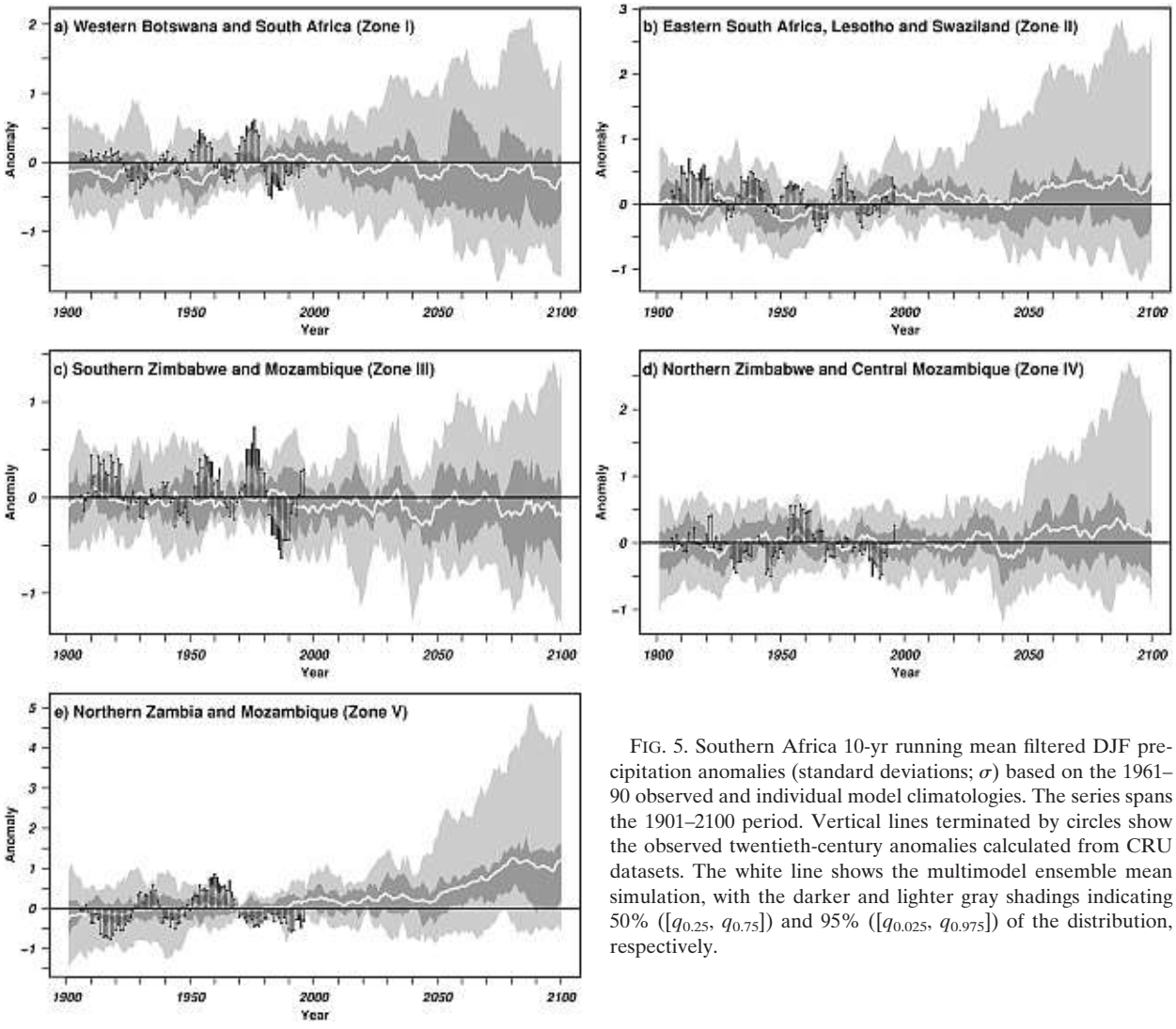

FIG. 5. Southern Africa 10-yr running mean filtered DJF precipitation anomalies (standard deviations; σ) based on the 1961–90 observed and individual model climatologies. The series spans the 1901–2100 period. Vertical lines terminated by circles show the observed twentieth-century anomalies calculated from CRU datasets. The white line shows the multimodel ensemble mean simulation, with the darker and lighter gray shadings indicating 50% ($[q_{0.25}, q_{0.75}]$) and 95% ($[q_{0.025}, q_{0.975}]$) of the distribution, respectively.

in Fig. 5. In these plots, high frequency variability has been filtered out using a 10-yr running mean. Without exception, low frequency modes of variability have dominated southern African rainfall during the last century. Such low-frequency rainfall fluctuations characterized by ~18 yr cycle have long been noted in southern African climate variability (Tyson et al. 1975). Decadal variability is seen to continue in the future although the spread in the model projections increases. Unlike here, where the models are equally weighted, the outliers [e.g., the GCM3.1 (T47) and Centre National de Recherches Météorologiques Coupled Global Climate Model, version 3 (CNRM-CM3) models for DJF] causing the observed large spread are downweighted by the Bayesian method in Figs. 3, 4, and 7. In most cases, the Bayesian weighting reduces the spread by more than a factor 2. Notwithstanding the large spread, some future patterns emerge. A notable upward trend is projected by a large fraction of the multimodel ensemble over northern Zambia, Mozambique, and Malawi (Fig. 5e). This upward trend is steeper after 2050. A similar albeit weaker trend is simulated in eastern South Africa (Fig. 5b). On the other hand, a tendency for drier seasons is projected in western Botswana and South Africa (Fig. 5a), particularly toward the end of the present century. In this subregion, the drying is stronger in the twenty-second century (not shown).

Apart from the late onset and early cessation signals (Fig. 3), internal decadal variability of rainfall in southern Africa remains large and is likely to mask any systematic changes in the total rainfall up to at least 2050.

4. Projected changes in atmospheric large-scale features

Given the statistical significance of the projected precipitation changes presented in foregoing sections, an important question is whether associated atmospheric anomalies can be identified. Previous studies that have reported on atmospheric (Mulenga et al. 2003) and oceanic anomalies (e.g., Rocha and Simmonds 1997a) associated with southern African precipitation anomalies. Motivated by these findings, we expect that atmospheric adjustments to perturbed radiative forcing will set up anomalous circulation, hence precipitation, patterns.

In a vast majority of studies, sea surface temperature (SST) anomalies in the tropical oceans (remote and adjacent) have been blamed for southern African seasonal rainfall anomalies by generally locking atmospheric flow patterns into particular regimes (Rocha and Simmonds 1997b; Cook 2001). SST anomalies in the subtropical oceans are also very important for southern Africa (Reason and Mulenga 1999; Behera and Yamagata 2001; Reason 2002). However, the correlation of African rainfall with SST is less than 0.4 almost everywhere, implying that a large percentage of rainfall variance is due to other sources. There is growing evidence that the land surface can also exert an influence (opposing or reinforcing), mainly through feedback mechanisms (Douville et al. 2001; Douville 2002; Cook et al. 2006).

We postulate that the climate change signal will be communicated to the precipitation field through other components of the climate system (e.g., the ocean or land surface) and/or through an alteration in spatial structure and strength of atmospheric circulation regimes. These would in turn influence atmospheric moisture characteristics. Our hypothesis therefore is that future climate shifts will resemble interannual and decadal variability. On these premises, model results of flow patterns that would potentially influence rainfall anomalies in southern Africa are discussed. Smaller samples than in the foregoing sections are dictated by availability and/or quality of reanalysis fields used to make comparisons with model output. For daily model output, only shorter time slices (of about 20 years) are available on the PCMDI archive.

a. Future moisture characteristics in spring

The reduction in spring precipitation is indicative of a delay in the rainfall onset over almost the entire southern African region. A trend toward a later onset has been found in the late twentieth century over parts of southern Africa (Tadross et al. 2005). Our results show that these decreases are likely to continue in the future climate (2051–2200). We have shown here that an early cessation is likely in many parts of the study region. Motivated by the spatial coherence in the simulated changes, and by similar reasons as Tadross et al. (2005), the focus will be placed only on the SON season.

SON lower-tropospheric (below 500-mb pressure level) horizontal moisture flux anomalies, $\mathbf{Q}'$, across southern Africa and the adjacent oceans have been calculated using daily CGCM simulations of specific humidity and the wind vector. This quantity is defined as

$$\mathbf{Q}' = \frac{1}{g}\int_{pt}^{pb} \langle q\mathbf{V}\rangle_f - \langle q\mathbf{V}\rangle_c dp, \tag{2}$$

where g is acceleration due to gravity, q is specific humidity, and $\mathbf{V}$ the wind vector. The integral is taken from the 1000-mb (p_b) to the 500-mb (p_t) pressure level. Angle brackets denote the time mean for future (f) and current (c) climate, here defined as the 1961–80 period. Positive SON precipitation anomalies (implying an early onset) occur more frequently around the latter years of the 1961–80 period, consistent with Tadross et al. (2005). Using this reference period should give an insight on the likely change in water vapor transport across southern Africa. We also compute anomalous moisture divergence, that is, $\nabla \cdot \mathbf{Q}'$.

Composite moisture transport fields for the driest minus wettest SON seasons are computed for each CGCM 1961–2000 simulation and displayed in the first column of Fig. 6. A dry (wet) season is defined whenever the amplitude of the first principal component standardized time score is less than (exceeds) one standard deviation. The composites are compared with the future (2046–65 and 2081–2100) moisture flux anomalies (second and third column of Fig. 6, respectively).

Evident in the composites are strong anomalous fluxes whereby moisture transported along the trades from the west Indian Ocean (north of ~20°S) is diverted north toward East Africa or is divergent (gray shading). To the south, the climatological onshore moisture transport is weakened or reversed. The CGCM dry anomalies are broadly similar with those computed from National Centers for Environmental Prediction–National Center for Atmospheric Research (NCEP–NCAR) reanalysis fields (not shown).

A selection of projected moisture flux anomalies is displayed in the last two columns of Fig. 6. The results from other models are broadly similar. A pattern of anomalous moisture divergence is found over a large part of the study region in most models. Furthermore, the anomaly patterns are characterized by well-organized anticyclonic anomalies over much of southeastern

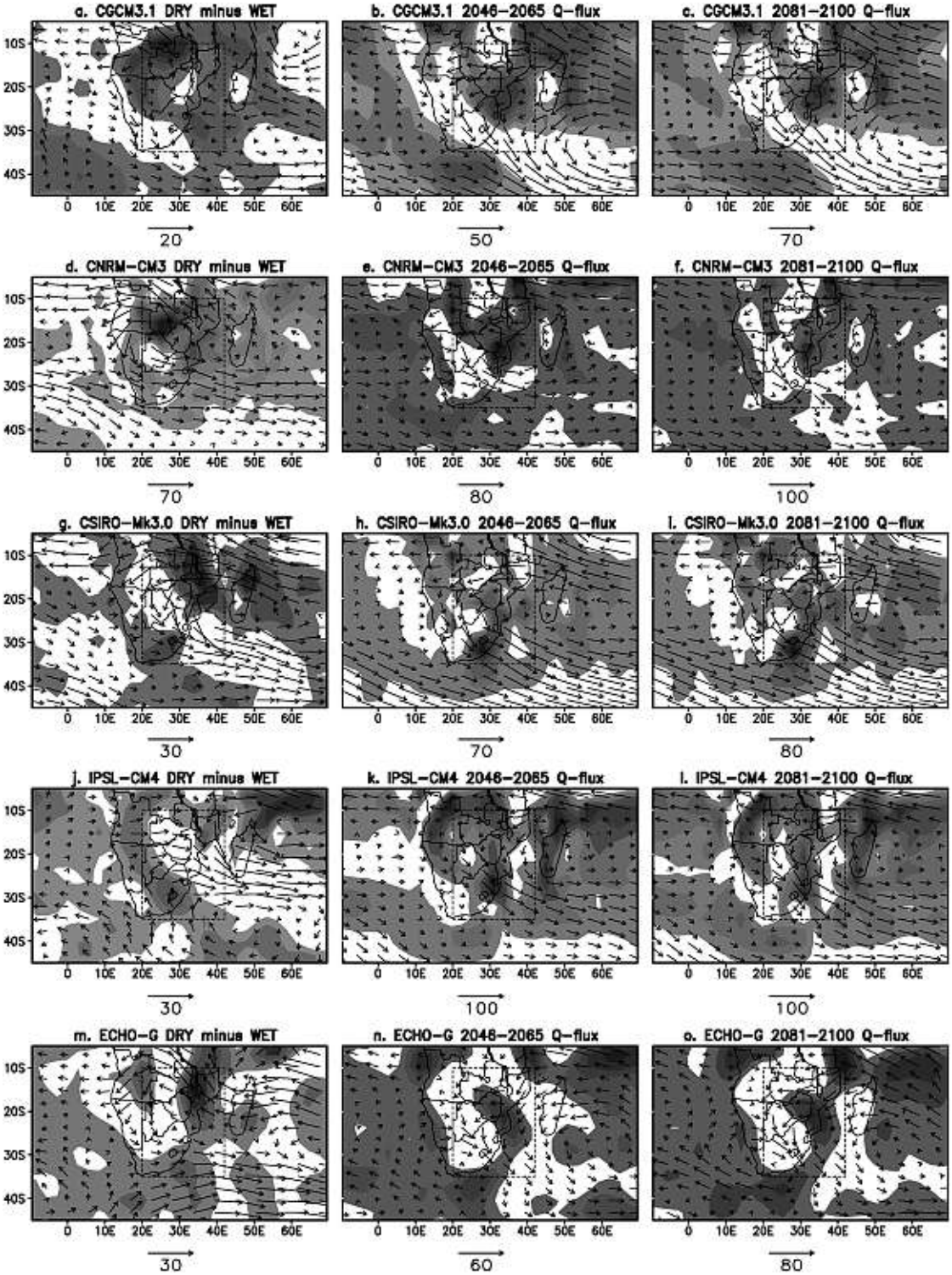

FIG. 6. SON lower-tropospheric horizontal moisture flux anomalies (kg m^{-1} s^{-1}). For each model (name given in the title), the first column displays composites of the driest minus wettest SON seasons during the 1961–2000 period. The middle and right columns show the 2046–65 and 2081–2100 moisture flux anomalies with respect to the 1961–80 period. Areas of moisture anomalous moisture divergence are shaded gray. Southern Africa (Fig. 1) is the land area in the dashed rectangular box.

Africa. Strong anomalous northwesterly moisture fluxes are found over the southwestern flank of the subtropical Indian Ocean anticyclone. This is indicative of a substantial weakening of moisture advection from the Indian Ocean into the subcontinent along the southeastern coast in future austral spring seasons, consistent with reduced precipitation. Westerlies from the southeast Atlantic are known to be cold and dry (due to cold waters and less evaporation; Mulenga et al. 2003). These are similar to the ones in the first column, showing that, indeed, the patterns of climate change resemble those of interannual and decadal variability in this respect.

It is quite likely that lower-tropospheric westerly anomalies along the southern latitudes in the models are dynamically coupled to a significant strengthening and equatorward expansion of the climatological upper-tropospheric westerlies associated with the Southern Hemisphere subtropical jet (SHSTJ). A striking similarity in the pattern of change in strength and latitudinal extent of the spring SHSTJ across the models used here has been found (not shown). Our results show that the boundary of the climatological westerly flux is likely to shift equatorward in future springs. In the western Indian Ocean north of ~10°S, the easterly monsoonal circulation carrying moisture gains a southerly component that diverts moisture into East Africa close to the equator. These are similar to the ones in the first column, showing that climate change patterns resemble those of interannual and decadal variability. From this one may draw two conclusions: First, dry spring seasons in the models (and in observations) are unambiguously generated by weaker lower-tropospheric moisture transport inland. Second, large-scale circulation changes, whereby moisture influx into southern Africa is substantially reduced (i.e., a decrease in moisture flux convergence), are a possible cause for the late rainfall onset in the future.

Surface and boundary layer processes would be another potential forcing mechanism for delayed rainfall onset. Evidence in support of drier winters in southern Africa in the future climate is presented in Fig. 7, consistent with previous findings (Solomon et al. 2007). Everywhere in the southern African domain, a statistically significant (at the 1% level everywhere but 5% level to the north) reduction in winter precipitation is simulated. The mean reduction in winter precipitation ranges from just under 20% to ~45%. Based on these projections, the delay in rainfall onset could in part be attributable to a drier land surface from the previous winter. Preseason anomalously wet soils have been identified to be a precursor to early seasonal rainfall onset (Reason et al. 2005). Reduced local evaporation and weaker lower-tropospheric moisture advection would

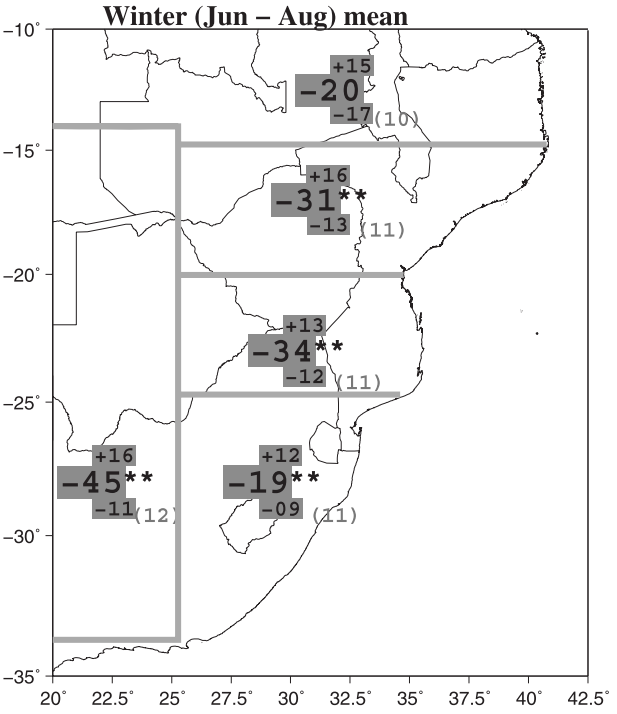

FIG. 7. As in Fig. 3, but for austral winter (Jun–Aug) mean precipitation rates.

possibly work in concert to delay the rainfall onset in southern Africa. However, moisture advection is a more significant source over most of southern Africa in spring as recycling ratios have been found to be low (Trenberth 1999). We note that a negative feedback mechanism whereby wetter soils would result in a concurrent net reduction in summer precipitation over southern Africa has been presented (Cook et al. 2006). A similar argument (negative feedback) whereby reduced local moisture recycling led to enhanced moisture advection and precipitation in some parts of southern Africa has been presented for the summer (November–February) 1998/99 season (New et al. 2003).

b. The tropical–temperate trough system

A seasonal northwest–southeast-oriented cloud band across southern Africa, stretching from the southeast Atlantic to the southwest Indian Ocean, has been identified as the major rainfall-bearing system during austral summer months (Kuhnel 1989). This feature, associated with a tropical–temperate trough (TTT) coupling system (Washington and Todd 1999), links tropical convection to midlatitude transient eddies and provides a mechanism for energy and moisture transport across the southern African middle troposphere (Todd et al. 2004). Owing to the important implications for southern Africa summer precipitation, using the daily model

precipitation simulations for the 2046–65 and 2081–2100 time slices, the likely behavior of this system is investigated.

The principal spatial mode of southern African DJF precipitation variability in the model simulations is identified from their empirical orthogonal functions (EOFs) (van den Dool 2007). The correlation matrix forms input into the EOF analysis. Consistent with Washington and Todd (1999), the spatial modes, while broadly similar in each summer month, are not identical. In the interest of brevity, we present the results for the leading January (center of the principal rainy season) unrotated EOFs and for a selection of models. Varimax-rotated EOFs have also been calculated. However, contrary to what one would expect from Buel patterns, the unrotated EOFs do not show uniform centered loadings of the same sign.

The first EOF loadings, expressed as the correlation ($\times$ 100) between their coefficient time series and the CGCM time series for each grid, are shown in Fig. 8. The EOF spatial fields are characterized by a northwest–southeast orientated dipole or tripole pattern. Evident in the spatial fields are loadings of opposite signs between locations south of the latitudinal band about 15°–20°S and those farther north and the southwest Indian Ocean. As expected, intermodel differences in the spatial extent and magnitudes of the EOF weights exist. Notwithstanding, the spatial patterns of simulated rainfall variability are broadly similar to those found in observations and coincide with preferred locations of the TTT (Washington and Todd 1999). The location of TTT, related to the south Indian Ocean convergence zone (SICZ), has been found to respond to ENSO-related SST anomalies (Cook 2000), particularly to west Indian Ocean SST forcing (Goddard and Graham 1999). The presence of this pattern of rainfall variability in the CGCM simulations suggests that the climate change signal might propagate into southern African precipitation through similar pathways as those communicating the interannual variability forcing.

Having realized that the models adequately capture the major rain-bearing system across southern Africa, the most relevant question for the present study is how frequent and persistent would the TTT be over the band of preferred locations? This would attempt to explain the dipole response in mean and extreme DJF precipitation (cf. Fig. 4) between the southwestern and northern areas of the domain (zones I and V, respectively). We endeavor to answer this question using the first EOF temporal coefficients displayed in Fig. 9. Positive standardized scores are indicative of periods when the TTT relocates northeastward (positive EOF weights in Fig. 8), and vice versa for negative scores (i.e., southwestward relocation). In a majority of cases, within each given January, the TTT propagates from the western pole northeastward into the southwest Indian Ocean. In a number of cases, the tropical–temperate rainband maintains its eastern locations throughout the month and in consecutive years. The presence of low frequency variability notwithstanding, there are indications for a higher frequency of positive scores in the Meteorological Research Institute (MRI) Coupled General Circulation Model, version 2.3.2 (CGCM2.3.2a) and Geophysical Fluid Dynamics Laboratory (GFDL) Climate Model version 3.1 (CM3.1) CGCMs (histograms not shown). However, the absence of a notably higher frequency in the other models inhibits us from drawing firm conclusions from our analysis.

5. Discussion and conclusions

The present study uses monthly data from the CMIP3 multimodel dataset to estimate likely changes in southern Africa precipitation. We have chosen model projections driven by the intermediate SRES A1b scenario, a standard emission scenario in which no drastic reduction of CO_2 emissions up to 2100 exists, after which the levels stay constant. This scenario has been chosen because it is realistic and offers 100 or 200 years of integrations with constant greenhouse gas levels at twice the preindustrial values. Based on the model projections, we have been able to estimate the likely change in intensity of mean and extreme precipitation at much smaller spatial scales than in previous studies. Within southern Africa, spatial inhomogeneities in the projected changes exist. The inhomogeneities are explained by the highly variable local forcing, modulating the large-scale signal. This is despite the fact that accurate representation of land surface features in the low-resolution models used here has not been achieved yet.

The uncertainty associated with these projections has been presented. Regions where and periods during which the modeled changes in precipitation show notable similarities between the GCMs have been identified, as well as regions where (and seasons when) marked differences are found. The similarity and spatial coherence of the modeled response to enhanced greenhouse gas forcing suggest a realistic and robust climate change signal. On the other hand, uncertainties characterize those regions where divergences in the modeled precipitation response are found as well as where systematic biases in the modeled twentieth-century climate exist. Such cases manifest in the form of a wide range of the projected changes.

A delay in rainy season onset has been found in southern Africa. We have identified two factors that are likely to contribute to this: First, a reduction in moisture

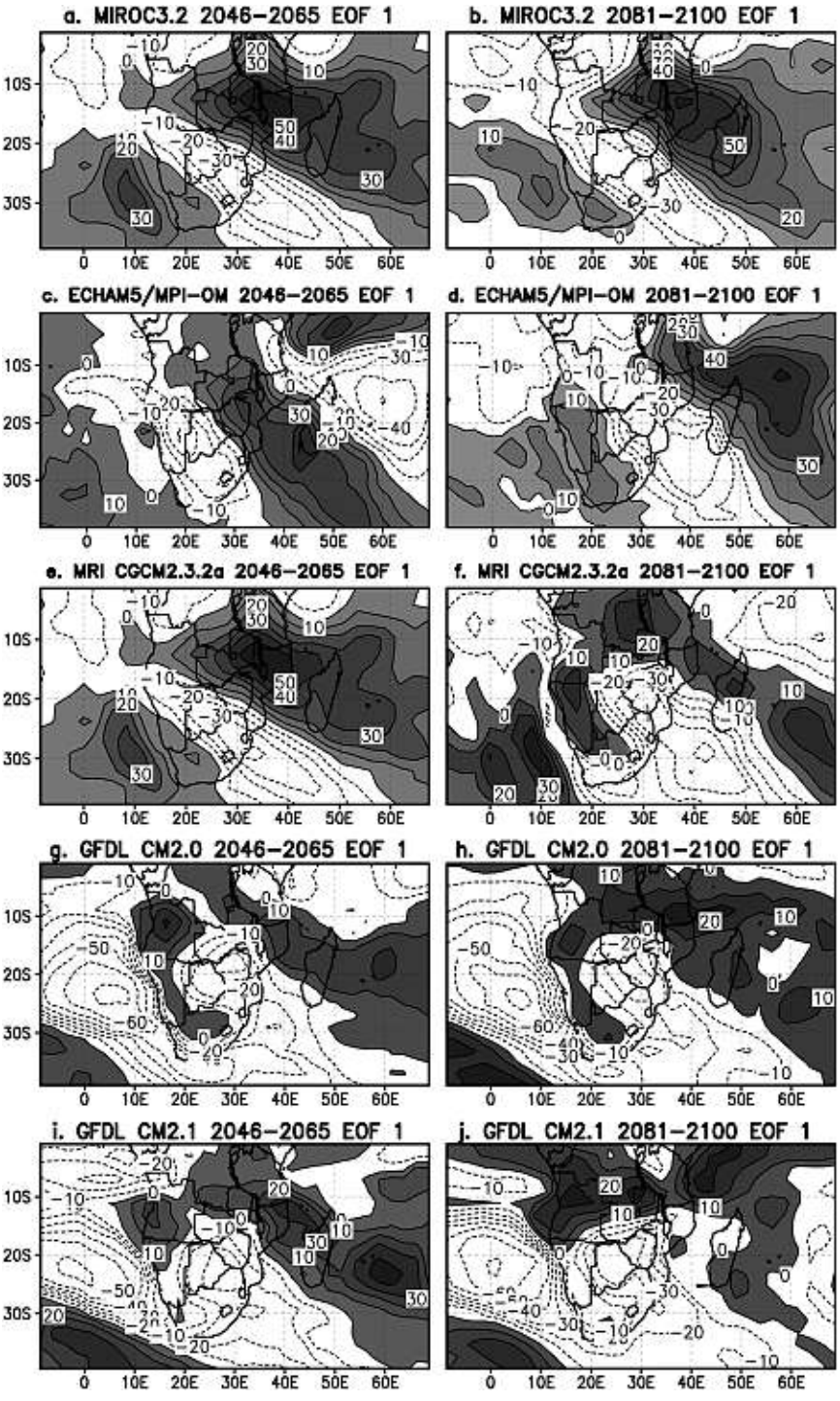

FIG. 8. January CGCM simulated precipitation EOF weights for the leading mode. For each model (name given in the title), the EOF weights for the 2046–65 and 2081–2100 January precipitation are given in the first and second columns, respectively.

influx into southern Africa. We have shown here that projected patterns of moisture transport are anomalously divergent over much of southern Africa. To the north flank of the south Indian Ocean anticyclone moisture is transported northwestward into East Africa. Over the southeastern parts, a reduction in moisture flux from the southwest Indian Ocean is found. Climate features forcing the large-scale circulation, and hence water

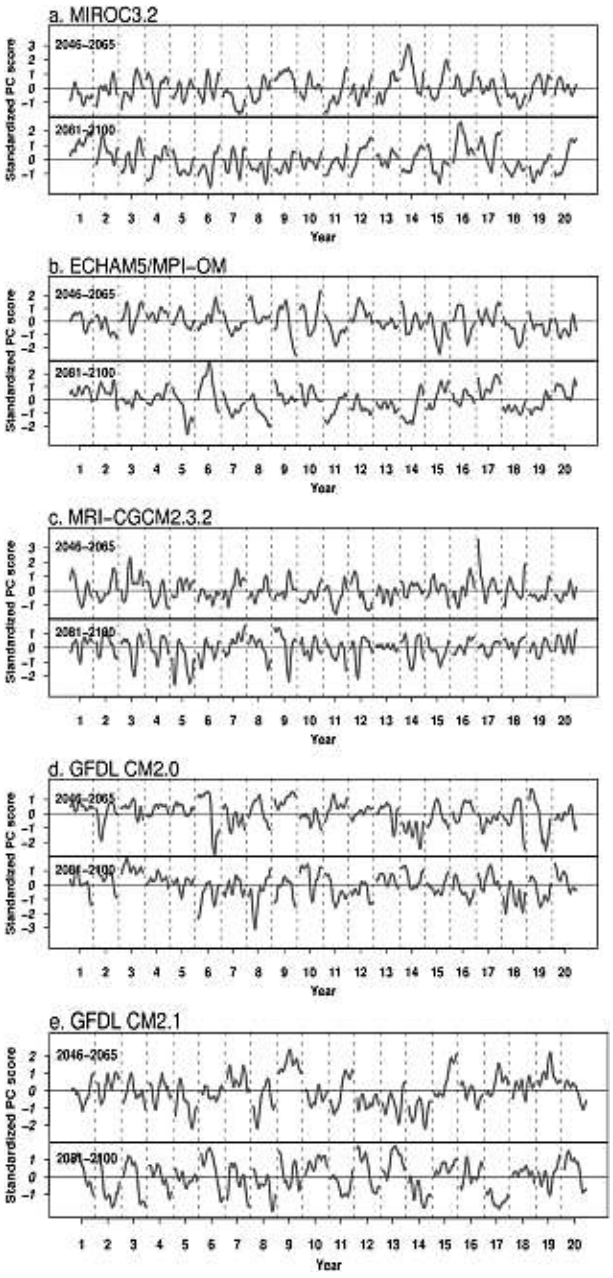

FIG. 9. Standardized principal component scores for each model simulated January daily precipitation. Each figure displays the 5-day running mean filtered scores for the 2046–65 (top row) and 2081–2100 (bottom row) time slice.

vapor transport changes, deserve further research attention. Second, preseason soil moisture deficits resulting in reduced local evaporation. Despite the low spring moisture recycling found in observations and modeling results showing a negative feedback from the land surface (soil moisture anomalies) in summer, drier soils would potentially reinforce lack of moisture for precipitation in future austral spring seasons.

In many parts of southern Africa, an early cessation of the rainy season is found. Possible causes of the earlier withdrawal of seasonal rains have not been investigated in this paper. This is a subject for future research. Our results point to a possible contraction in the rainfall season in locations south of about 15°S. To the north, the rainy season is projected to shift to later months (i.e., a late start and a delayed cessation).

Mean summer precipitation rates are projected to decrease near the hyperarid and semiarid areas of southern Africa (zone I). Over these areas, the severity of future droughts is projected to increase. North of about 15°S, mean summer precipitation is projected to increase. Although no causal relationship is implied, more frequent west Indian Ocean positioned tropical–temperate cloud bands are consistent with a reduction in summer precipitation rates and more severe droughts to the southwest.

Wet events are projected to become more intense to the north and southeast. To the north, this is consistent with more prolonged wet spells from persistent convective activity related to the TTT. The increase in the intensity of wettest events to the southeast is in qualitative agreement with Hewitson and Crane (2006). These increases in wet extremes may exacerbate the rise in reported flood disasters in the region. We note, however, that future projections of wettest events are less trustworthy owing to the inability to accurately simulate small-scale disturbances such as west Indian Ocean tropical cyclone activity in most models.

In general, the pattern of summer precipitation change, in particular coupled with increasing temperatures, may result in an eastward extension of desert areas in southern Africa, water scarcity, reduced agricultural productivity, and increased risks of food insecurity and famine. Not only is desertification a potential impact of global warming in southern Africa, but shorter growing seasons are possible consequences in a large area.

Acknowledgments. This research has been funded by the Dutch Ministry of Foreign Affairs, Development Cooperation. CASC was supported by ENSEMBLES (GOCE-CT-2003-505539), and Fundacão de Amparo a Pesquisa do Estado de São Paulo (FAPESP), Processes 2005/05210-7 and 2006/02497-6. Claudia Tebaldi provided the MCMC algorithm used in this work. Review comments by Rein Haarsma, Chris Reason, Claudia Tebaldi, and two anonymous reviewers significantly improved the original manuscript.

Technical contributions by Henk van den Brink towards the success of this study are gratefully acknowledged. We acknowledge the modeling groups, the Program for Climate Model Diagnosis and Intercomparison

(PCMDI) and the WCRP's Working Group on Coupled Modelling (WGCM) for their roles in making available the WCRP CMIP3 multimodel dataset. Support of this dataset is provided by the Office of Science, U.S. Department of Energy.

APPENDIX A

Methodology Used in Extreme Value Analysis

The peak-over-threshold method or generalized Pareto distribution has been used as the extreme value model in this study. We follow the approach described by Coles (2001). In this approach, a threshold intensity u is determined a priori. The data exceeding the threshold (z: $z > u$) are then fitted to a GPD, defined as

$$G(z;\ \sigma,\ \xi,\ u) = \begin{cases} 1 - \left(1 + \dfrac{\xi(z-u)}{\sigma}\right)^{-1/\xi}, & \xi \neq 0 \\ 1 - e^{-(z-u)/\sigma}, & \xi = 0, \end{cases} \tag{A1}$$

where $\sigma > 0$ and ξ are the scale and shape parameters of the distribution, respectively, such that

$$1 + \frac{\xi(z-u)}{\sigma} > 0.$$

This distribution gives the probability that a random variable z is higher than a high value conditional on it exceeding the predefined threshold u.

In this study, we set the threshold to the 80th percentile for the wet extremes to ensure an adequate number of excesses and a sufficiently small variance in the estimated model parameters. For dry extremes, the data are subjected to a negative transformation, and the excesses are defined analogously. For climate models with m integrations, each ensemble member is considered as an independent realization. The ensemble members are then concatenated to form a larger sample. This specification has allowed $m \times 20$ ($m \times 30$) exceedances in the control (future) climate record of 100 (150) years. However, in certain cases, notably when $m > 1$, the quality of the GPD fit, as assessed using an Anderson-Darling test (see below), was poor. Guided by the mean residual life plot (Coles 2001), the threshold was then adjusted to improve the quality of the fit.

The GPD parameters (i.e., α and ξ) have been estimated using maximum likelihood. The estimated parameters are then used to in the quantile function used to calculate the return level z_p. The return level z_p is that level which has probability p of being exceeded in a given year, or, defined differently, the level likely to be exceeded once every $1/p$ years. Based on Eq. (A1), it is given by

$$z_p = \begin{cases} u + \dfrac{\sigma}{\xi}[(p\zeta_u)^{\xi} - 1], & \xi \neq 0 \\ u + \sigma\log(p\zeta_u), & \xi = 0. \end{cases} \tag{A2}$$

The quantity ζ_u gives the probability of exceeding the predefined threshold and has a variance approximately $\zeta_u(1 - \zeta_u)/n$. This follows from the argument that in a sample of size n, the number of threshold exceedances (n_u) has a binomial distribution [i.e. $n_u \sim \text{bin}(n, \zeta_u)$]. The uncertainties in the estimates of $\zeta_u \approx n_u/n$, σ, and ξ are incorporated in estimating the uncertainty associated with the estimate of z_p. This is achieved using the variance–covariance matrix for (ζ_u, σ, ξ), given by

$$\mathbf{V} = \begin{bmatrix} \text{var}(\zeta_u) & 0 & 0 \\ 0 & \dfrac{\partial^2 l(\theta)}{\partial\sigma^2} & \dfrac{\partial^2 l(\theta)}{\partial\sigma\partial\xi} \\ 0 & \dfrac{\partial^2 l(\theta)}{\partial\sigma\partial\xi} & \dfrac{\partial^2 l(\theta)}{\partial\xi^2} \end{bmatrix}. \tag{A3}$$

Here $v_{12} = v_{21} = \text{cov}(\zeta_u, \sigma)$; $v_{31} = v_{13} = \text{cov}(\zeta_u, \xi)$; $v_{23} = v_{32} = \text{cov}(\sigma, \xi)$; $v_{22} = \text{var}(\sigma)$; $v_{33} = \text{var}(\xi)$. In each case, the partial derivatives of the likelihood function [$l(\theta)$] are evaluated at the estimated GPD parameters.

The standard error in the estimate of z_p is obtained from the square root of var(z_p), given by

$$\text{var}(z_p) = \left[\frac{\partial z_p}{\partial\zeta_u}, \frac{\partial z_p}{\partial\sigma}, \frac{\partial z_p}{\partial\xi}\right]^T \begin{bmatrix} \text{var}(\zeta_u) & 0 & 0 \\ 0 & \dfrac{\partial^2 l(\theta)}{\partial\sigma^2} & \dfrac{\partial^2 l(\theta)}{\partial\sigma\partial\xi} \\ 0 & \dfrac{\partial^2 l(\theta)}{\partial\sigma\partial\xi} & \dfrac{\partial^2 l(\theta)}{\partial\xi^2} \end{bmatrix} \left[\frac{\partial z_p}{\partial\zeta_u}, \frac{\partial z_p}{\partial\sigma}, \frac{\partial z_p}{\partial\xi}\right]. \tag{A4}$$

The $100(1 - \alpha)\%$ confidence interval of z_p is then expressed as

$$z_p \pm Z_{\alpha/2}\sqrt{\text{var}(z_p)}, \tag{A5}$$

where $Z_{\alpha/2}$ is the $(1 - \alpha/2)\%$ point of the standard normal distribution. The return levels estimated from this approach have Gaussian likelihoods, which conforms with the requirement of the Bayesian multimodel ensembling method used in this study (see Tebaldi et al. 2005).

APPENDIX B

Goodness-of-Fit Tests

Prior to estimating the return level z_p, Anderson-Darling goodness-of-fit tests have been performed. In this test, a quadratic measure of the discrepancies between the fitted and empirical cumulative distribution functions (CDF), weighted by $[G(z)(1 - G(z))]^{-1}$ is expressed as

$$A^2 = n_u \int_{z:z>u}^{z_{nu}} [G_{n_u}(z) - G(z)]^2 [G(z)(1 - G(z))]^{-1} dG(z). \tag{B1}$$

In this way, discrepancies occurring at the tails are weighted more than those in the central part of the distribution. The empirical CDF $G_{n_u}(z)$ is calculated using

$$G_{n_u}(z) = \begin{cases} 0, & z < u \\ \dfrac{i}{n_u}, & z_i \le z < z_{i+1}, \quad i = 1, \ldots, n_u - 1 \\ 1, & z = z_{n_u}, \end{cases} \tag{B2}$$

Conventionally, the test statistic is estimated by

$$A^2 = -n_u - \sum_{i=1}^{n_u} \frac{2i - 1}{n_u} [\log G(z) + \log(1 - G(z_{n_u+1-i}))]. \tag{B3}$$

The null hypothesis—that the data exceeding the predefined threshold (u) has a generalized Pareto distribution—is rejected whenever the test statistic value exceeds the critical value at the specified level of significance (i.e., one-sided test).

REFERENCES

Behera, S. K., and T. Yamagata, 2001: Subtropical SST dipole events in the southern Indian Ocean. *Geophys. Res. Lett.,* **28,** 327–330.

Coles, S., 2001: *An Introduction to Statistical Modeling of Extreme Values*. Springer, 208 pp.

Cook, B., G. B. Bonan, and S. Levis, 2006: Soil moisture feedbacks to precipitation in southern Africa. *J. Climate,* **19,** 4198–4206.

Cook, K. H., 2000: The south Indian convergence zone and interannual variability over southern Africa. *J. Climate,* **13,** 3789–3804.

——, 2001: A Southern Hemisphere wave response to ENSO with implications for southern Africa precipitation. *J. Atmos. Sci.,* **58,** 2146–2162.

Delworth, T. L., and Coauthors, 2006: GFDL's CM2 global coupled climate models. Part I: Formulation and simulation characteristics. *J. Climate,* **19,** 643–674.

Douville, H., 2002: Influence of soil moisture on the Asian and African monsoons. Part II: Interannual variability. *J. Climate,* **15,** 701–720.

——, F. Chauvin, and H. Broqua, 2001: Influence of soil moisture on the Asian and African monsoons. Part I: Mean monsoon and daily precipitation. *J. Climate,* **14,** 2381–2403.

Flato, G. M., cited 2005: The third generation coupled global climate model (CGCM3). [Available online at http://www.cccma.ec.gc.ca/models/cgcm3.shtml.]

Giorgi, F., and R. Francisco, 2000: Uncertainties in regional climate change predictions. A regional analysis of ensemble simulations with the HADCM2 GCM. *Climate Dyn.,* **16,** 169–182.

——, and L. O. Mearns, 2002: Calculation of average, uncertainty range, and reliability of regional climate changes from AOGCM simulations via the ''reliability ensemble average'' (REA) method. *J. Climate,* **15,** 1141–1158.

——, and ——, 2003: Probability of regional climate change based on reliability ensemble average (REA) method. *Geophys. Res. Lett.,* **30,** 1629, doi:10.1029/2003GL017130.

Goddard, L., and N. E. Graham, 1999: The importance of the Indian Ocean for simulating rainfall anomalies over eastern and southern Africa. *J. Geophys. Res.,* **104,** 19 099–19 116.

Gordon, C., C. Cooper, C. Senior, H. Banks, J. Gregory, T. Johns, J. Mitchell, and R. Wood, 2000: The simulation of SST, sea ice extents and ocean heat transports in a version of the Hadley Centre coupled model without flux adjustments. *Climate Dyn.,* **16,** 147–168.

Gordon, H. B., and Coauthors, 2002: The CSIRO Mk3 climate system model. Tech Research Paper 60, CSIRO Atmospheric Research, Aspendale, Victoria, Australia, 130 pp.

Groisman, P. Ya., R. W. Knight, D. R. Easterling, T. R. Karl, G. C. Hegerl, and V. N. Razuvaev, 2005: Trends in intense precipitation in the climate record. *J. Climate,* **18,** 1326–1350.

Hasumi, H., and Coauthors, 2004: K-1 technical report. Tech. Rep. 1, CCSR/NIES/FRCGC, Meguro-ku, Tokyo, Japan, 34 pp.

Hellmuth, M. E., A. Moorhead, M. C. Thomson, and J. Williams, Eds., 2007: *Climate Risk Management in Africa: Learning from Practice*. International Research Institute for Climate and Society (IRI), 116 pp.

Hewitson, B. C., and R. G. Crane, 2006: Consensus between GCM climate change projections with empirical downscaling: Precipitation downscaling over South Africa. *Int. J. Climatol.,* **26,** 1315–1337.

Houghton, J. T., Y. Ding, D. J. Griggs, M. Noguer, P. J. van der Linden, X. Dai, K. Maskell, and C. A. Johnson, Eds., 2001: *Climate Change 2001: The Scientific Basis*. Cambridge University Press, 881 pp.

Hulme, M., R. Doherty, T. Ngara, M. New, and D. Lister, 2001: African climate change: 1900–2100. *Climate Res.,* **17,** 145–168.

Johns, T., and Coauthors, 2004: HadGEM1 model description and analysis of preliminary experiments for the IPCC Fourth Assessment Report. Tech. Note 55, Met Office, Exeter, United Kingdom, 75 pp.

Johnson, R. A., and D. W. Wichern, 2002: *Applied Multivariate Statistical Analysis*. Prentice Hall, 767 pp.

Joubert, A. M., S. J. Mason, and J. S. Galpin, 1996: Droughts over southern Africa in a doubled-CO_2 climate. *Int. J. Climatol.,* **16,** 1149–1156.

Kharin, V. V., and F. W. Zwiers, 2000: Changes in the extremes in an ensemble of transient climate simulations with a coupled atmosphere–ocean GCM. *J. Climate,* **13,** 3760–3788.

——, ——, X. Zhang, and C. Hegerl, 2007: Changes in temperature and precipitation extremes in the IPCC ensemble of global coupled model simulations. *J. Climate,* **20,** 1419–1444.

Kuhnel, I., 1989: Tropical–extratropical cloudband climatology. *Int. J. Climatol.,* **9,** 441–463.

Laio, F., 2004: Cramer–von Mises and Anderson-Darling goodness of fit tests for extreme value distributions with unknown parameters. *Water Resour. Res.,* **40,** W09308, doi:10.1029/2004WR003204.

Le Clainche, Y., P. Braconnot, O. Marti, S. Joussaume, J.-L. Dufresne, and M.-A. Filiberti, 2001: The role of sea ice thermodynamics in the Northern Hemisphere climate as simulated by a global coupled ocean-atmosphere model. Notes du Pôle de Modération 21, Institut Pierre Simon Laplace, Paris, France, 26 pp.

Mason, S. J., P. R. Waylen, G. M. Mimmack, B. Rajaratnam, and J. M. Harrison, 1999: Changes in extreme rainfall events in South Africa. *Climate Change,* **41,** 249–257.

Meehl, G. A., J. M. Arblaster, and C. Tebaldi, 2005: Understanding future patterns of increased precipitation intensity in climate model simulations. *Geophys. Res. Lett.,* **32,** L18719, doi:10.1029/2005GL023680.

Mimmack, G. M., S. J. Mason, and J. S. Galpin, 2001: Choice of distance matrices in cluster analysis: Defining regions. *J. Climate,* **14,** 2790–2797.

Min, S.-K., S. Legutke, A. Hense, and W.-T. Kwon, 2005: Internal variability in a 1000-yr control simulation with the coupled climate model ECHO-G I. Near-surface temperature, precipitation and mean sea level pressure. *Tellus,* **57A,** 605–621.

Mulenga, H. M., M. Rouault, and C. J. C. Reason, 2003: Dry summers over NE South Africa and associated circulation anomalies. *Climate Res.,* **25,** 29–41.

New, M., M. Hulme, and P. Jones, 2000: Representing twentieth-century space–time climate variability. Part II: Development of 1901–96 monthly grids of terrestrial surface climate. *J. Climate,* **13,** 2217–2238.

——, R. Washington, C. Jack, and B. Hewitson, 2003: Sensitivity of southern Africa climate to soil-moisture. *Clivar Exchanges,* No. 8, International CLIVAR Project Office, Southampton, United Kingdom, 45–47.

——, and Coauthors, 2006: Evidence of trends in daily climate extremes over southern and west Africa. *J. Geophys. Res.,* **111,** D14102, doi:10.1029/2005JD006289.

Peterson, T. C., H. Daan, and P. D. Jones, 1997: Initial selection of a GCOS surface network. *Bull. Amer. Meteor. Soc.,* **78,** 2145–2152.

Reason, C. J. C., 2002: Sensitivity of the southern African circulation to dipole SST patterns in the South Indian Ocean. *Int. J. Climatol.,* **22,** 377–393.

——, 2007: Tropical cyclone Dera, the unusual 2000/01 tropical cyclone season in the southwest Indian Ocean and associated rainfall anomalies over southern Africa. *Meteor. Atmos. Phys.,* **97,** 181–188.

——, and H. M. Mulenga, 1999: Relationships between South African rainfall and SST anomalies in the southwest Indian Ocean. *Int. J. Climatol.,* **19,** 1651–1673.

——, and I. Keibel, 2004: Tropical Cyclone Eline and its unusual penetration and impacts over the southern African mainland. *Wea. Forecasting,* **19,** 789–805.

——, S. Hachigonta, and R. F. Phaladi, 2005: Interannual variability in rainy season characteristics over the Limpopo region of southern Africa. *Int. J. Climatol.,* **25,** 1835–1853.

Rocha, A., and I. Simmonds, 1997a: Interannual variability of south-eastern African summer rainfall. Part 1: Relationships with air-sea interaction processes. *Int. J. Climatol.,* **17,** 235–265.

——, and ——, 1997b: Interannual variability of south-eastern African summer rainfall. Part 2: Modelling the impact of sea-surface temperatures on rainfall and circulation. *Int. J. Climatol.,* **17,** 267–290.

Roeckner, E., and Coauthors, 2003: The atmospheric general circulation model ECHAM5. Tech. Rep. 349, Max-Planck-Institut für Meteorologie, Hamburg, Germany, 140 pp.

Ropelewski, C. F., and M. S. Halpert, 1987: Global and regional scale precipitation patterns associated with the El Niño/Southern Oscillation. *Mon. Wea. Rev.,* **115,** 1606–1626.

Rouault, M., S. A. White, C. J. C. Reason, J. R. E. Lutjeharms, and I. Jobard, 2002: Ocean–atmosphere interaction in the Agulhas Current region and a South African extreme weather event. *Wea. Forecasting,* **17,** 655–669.

Salas-Mélia, D., and Coauthors, 2005: Description and validation of the CNRM-CM3 global coupled model. CNRM Working Note 103, 36 pp.

Shongwe, M. E., W. A. Landman, and S. J. Mason, 2006: Performance of recalibration systems for GCM forecasts for southern Africa. *Int. J. Climatol.,* **17,** 1567–1585.

——, G. J. van Oldenborgh, B. J. J. M. van den Hurk, and M. van Aalst, 2008: Projected changes in mean and extreme precipitation in Africa under global warming. Part II: East Africa. *J. Climate,* submitted.

Solomon, S., D. Qin, M. Manning, M. Marquis, K. Averyt, M. M. B. Tignor, H. L. Miller Jr., and Z. Chen, Eds., 2007: *Climate Change 2007: The Physical Science Basis*. Cambridge University Press, 996 pp.

Tadross, M. A., B. C. Hewitson, and M. T. Usman, 2005: The interannual variability of the onset of the maize growing season over South Africa and Zimbabwe. *J. Climate,* **18,** 3356–3372.

Tebaldi, C., L. O. Mearns, D. Nychka, and R. L. Smith, 2004: Regional probabilities of precipitation change: A Bayesian analysis of multimodel simulations. *Geophys. Res. Lett.,* **31,** L24213, doi:10.1029/2004GL021276.

——, R. L. Smith, D. Nychka, and L. O. Mearns, 2005: Quantifying uncertainty in projections of regional climate change: A Bayesian approach to the analysis of multimodel ensembles. *J. Climate,* **18,** 1524–1540.

Todd, M. C., and R. Washington, 1999: Circulation anomalies associated with tropical-temperate troughs in southern Africa and the south-west Indian Ocean. *Climate Dyn.,* **15,** 937–951.

——, ——, and P. I. Palmer, 2004: Water vapour transport associated with tropical-temperate trough systems over southern Africa and the southwest Indian Ocean. *Int. J. Climatol.,* **24,** 555–568.

Trenberth, K. E., 1999: Atmospheric moisture recycling: Role of advection and local evaporation. *J. Climate,* **12,** 1368–1381.

——, A. Dai, R. M. Rasmussen, and D. B. Parsons, 2003: The changing character of precipitation. *Bull. Amer. Meteor. Soc.,* **84,** 1205–1217.

Tyson, P. D., and R. A. Preston-Whyte, 2000: *The Weather and Climate of Southern Africa*. Oxford University Press, 396 pp.

——, T. G. J. Dyer, and M. N. Mametse, 1975: Secular changes in South African rainfall: 1880 to 1972. *Quart. J. Roy. Meteor. Soc.,* **101,** 817–833.

van Aalst, M. K., M. Helmer, C. de Jong, F. Monasso, E. van Sluis, and P. Suarez, 2007: Red Cross/Red Crescent climate guide. Technical Rep., Red Cross/Red Crescent Climate Centre, The Hague, Netherlands, 73 pp.

van den Dool, H., 2007: *Empirical Methods in Short-Term Climate Prediction*. Oxford University Press, 215 pp.

van den Hurk, B. J. J. M., and Coauthors, 2006: KNMI climate change scenarios 2006 for the Netherlands. Tech. Rep. WR-2006-01, KNMI, 82 pp.

van Ulden, A. P., and G. J. van Oldenborgh, 2006: Large-scale atmospheric circulation biases and changes in global climate model simulations and their importance for climate change in Central Europe. *Atmos. Chem. Phys.,* **6,** 863–881.

Washington, R., and M. C. Todd, 1999: Tropical temperate links in southern Africa and southwest Indian Ocean daily rainfall. *Int. J. Climatol.,* **19,** 1601–1616.

——, and A. Preston, 2006: Extreme wet years over southern Africa: Role of Indian Ocean sea surface temperatures. *J. Geophys. Res.,* **111,** D15104, doi:10.1029/2005JD006724.

Yukimoto, S., and A. Noda, 2001: Improvements of the Meteorological Research Institute global ocean-atmosphere coupled GCM(MRI-CGCM2) and its climate sensitivity. CGER Supercomputer Activity Rep. 10, 37–44.